A Ras-induced conformational switch in the Ras activator Son of sevenless

Tanya S. Freedman*, Holger Sondermann*†, Gregory D. Friedland‡, Tanja Kortemme‡§, Dafna Bar-Sagi¶, Susan Marqusee*‖, and John Kuriyan*‖**††

*Department of Molecular and Cell Biology, California Institute for Quantitative Biomedical Research, **Department of Chemistry, and Howard Hughes Medical Institute, University of California, Berkeley, CA 94720; ‖Physical Biosciences Division, Lawrence Berkeley National Laboratory, Berkeley, CA 94720; ‡Graduate Group in Biophysics, §Department of Biopharmaceutical Sciences, and California Institute for Quantitative Biomedical Research, University of California, San Francisco, CA 94143; and ¶Department of Biochemistry, New York University School of Medicine, New York, NY 10016

Contributed by John Kuriyan, September 14, 2006

The Ras-specific guanine nucleotide-exchange factors Son of sevenless (Sos) and Ras guanine nucleotide-releasing factor 1 (RasGRF1) transduce extracellular stimuli into Ras activation by catalyzing the exchange of Ras-bound GDP for GTP. A truncated form of RasGRF1 containing only the core catalytic Cdc25 domain is sufficient for stimulating Ras nucleotide exchange, whereas the isolated Cdc25 domain of Sos is inactive. At a site distal to the catalytic site, nucleotide-bound Ras binds to Sos, making contacts with the Cdc25 domain and with a Ras exchanger motif (Rem) domain. This allosteric Ras binding stimulates nucleotide exchange by Sos, but the mechanism by which this stimulation occurs has not been defined. We present a crystal structure of the Rem and Cdc25 domains of Sos determined at 2.0-Å resolution in the absence of Ras. Differences between this structure and that of Sos bound to two Ras molecules show that allosteric activation of Sos by Ras occurs through a rotation of the Rem domain that is coupled to a rotation of a helical hairpin at the Sos catalytic site. This motion relieves steric occlusion of the catalytic site, allowing substrate Ras binding and nucleotide exchange. A structure of the isolated RasGRF1 Cdc25 domain determined at 2.2-Å resolution, combined with computational analyses, suggests that the Cdc25 domain of RasGRF1 is able to maintain an active conformation in isolation because the helical hairpin has strengthened interactions with the Cdc25 domain core. These results indicate that RasGRF1 lacks the allosteric activation switch that is crucial for Sos activity.

Cdc25 | nucleotide-exchange factor | crystal structure | Ras exchanger motif (Rem) domain | Ras guanine nucleotide-releasing factor 1

Ras is a critical signaling molecule that cycles between inactive GDP-bound and active GTP-bound states (1). The activation of Ras by receptor tyrosine kinases proceeds through the recruitment of the nucleotide-exchange factor Son of sevenless (Sos) to the plasma membrane, where it encounters Ras and stimulates release of GDP, allowing its replacement by GTP (2–6). In some cells, G protein-coupled receptors rely on relatives of Sos, such as Ras guanine nucleotide-releasing factor 1 (RasGRF1), also known as $p140^{Ras\text{-}GRF}$ or Cdc25, for initiating Ras signaling (7–12).

The region of Sos that is required for Ras-specific nucleotide-exchange activity, Sos^{cat}, contains a Ras exchanger motif (Rem) domain and a Cdc25 homology domain (Fig. 1*a*) (13, 14). In addition, Sos requires allosteric activation through a second Ras-binding site that bridges the Rem and Cdc25 domains (Fig. 1*b*) (15, 16). When Sos is activated, the Cdc25 domain of Sos inserts a helical hairpin (Fig. 1 and Fig. 7, which is published as supporting information on the PNAS web site) between two flexible regions of Ras, switch 1 and switch 2, opening the nucleotide-binding site of Ras for GDP release (14). Ras·GTP binds more tightly to the allosteric site than does Ras·GDP, leading to positive feedback on the initiation of nucleotide exchange (15, 16). Ras binding at the allosteric site has been shown to increase the affinity of Ras for the Sos catalytic site (16), but the structural basis for this allosteric activation has not been clear. In contrast to Sos, which requires Ras binding to the allosteric site for activity, the Cdc25 domain of RasGRF1 is active on its own (Fig. 1*b*) (11, 17).

To identify the conformational changes that accompany Sos activation we have determined the crystal structure of Sos^{cat}, containing the Rem and Cdc25 domains, in the absence of Ras at 2.0-Å resolution and that of the Cdc25 domain of RasGRF1, also without Ras bound, at 2.2-Å resolution. Comparison of these structures with that of Sos^{cat} bound to Ras (14, 15) reveals the switch by which allosteric Ras binding conveys an activating signal to the Sos catalytic site and the structural basis for RasGRF1 activity in the absence of allosteric activation.

Results and Discussion

Unlike RasGRF1, Sos Requires Allosteric Activation for Nucleotide Exchange Activity. We performed nucleotide-exchange assays in which we monitored the release rate of fluorescently labeled GDP from Ras in the presence and absence of nucleotide-exchange factor (11, 18). Guided by secondary structure prediction and sequence alignment to Sos (14, 19, 20), we created a construct of RasGRF1 that spans residues 1,028 to 1,262, $RasGRF1^{Cdc25}$, which is 51 residues shorter than that used in earlier biochemical studies (17). The rate of nucleotide release from Ras in the presence of $RasGRF1^{Cdc25}$ ($50 \pm 10 \times 10^{-4}$ s^{-1} for 1 μM exchange factor) is comparable to the value (100×10^{-4} s^{-1} for 1 μM exchange factor) reported previously (17) and is significantly higher than the intrinsic rate of nucleotide release by isolated Ras ($1.8 \pm 0.2 \times 10^{-4}$ s^{-1}; Fig. 2).

Sos^{cat} (Rem-Cdc25) displays a basal level of nucleotide-exchange activity attributable to allosteric activation by Ras·GDP, normally present as the substrate in nucleotide-exchange assays (16, 18). To minimize this interference, we used 0.1 μM substrate Ras·GDP, a concentration 10-fold lower than the substrate concentrations used in previous studies (16) and >100-fold lower than the value estimated for the dissociation constant (>25 μM) for Ras·GDP binding at the allosteric site of Sos (16). Under these conditions, the rate of nucleotide release

Author contributions: T.S.F. and H.S. contributed equally to this work; T.S.F., H.S., G.D.F., T.K., D.B.-S., S.M., and J.K. designed research; T.S.F., H.S., and G.D.F. performed research; T.S.F., H.S., G.D.F., and T.K. contributed new reagents/analytic tools; T.S.F., H.S., G.D.F., T.K., D.B.-S., S.M., and J.K. analyzed data; and T.S.F., H.S., G.D.F., T.K., and J.K. wrote the paper.

The authors declare no conflict of interest.

Freely available online through the PNAS open access option.

Abbreviations: Sos, Son of sevenless; RasGRF1, Ras guanine nucleotide-releasing factor 1; Rem, Ras exchanger motif; mant-dGDP, 3′-*O*-*N*-methyl-anthraniloyl-2′-deoxy-guanosine-5′-diphosphate.

Data deposition: The crystallographic coordinates and structure factors have been deposited in the Protein Data Bank, www.pdb.org (PDB ID codes 2II0 and 2IJE).

†Present address: Department of Molecular Medicine, College of Veterinary Medicine, Cornell University, Ithaca, NY 14853.

††To whom correspondence should be addressed. E-mail: kuriyan@berkeley.edu.

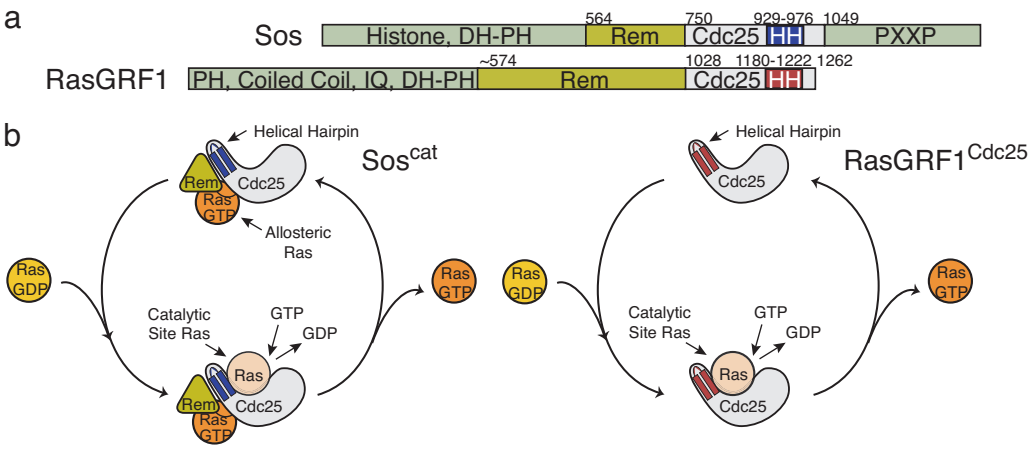

Fig. 1. Sos and RasGRF1 catalyze Ras nucleotide-exchange. (*a*) Domain structure of human Sos1 and murine RasGRF1. Sos and RasGRF1 both contain Rem domains (yellow) and Cdc25 homology domains (gray) that include a helical hairpin motif (HH; blue in Sos, red in RasGRF1). Together, the Sos Rem and Cdc25 domains are referred to as Sos^{cat}. Other domains in Sos and RasGRF1 contribute to localization and regulation: DH, Dbl homology; PH, pleckstrin homology; IQ, motif for Ca^{2+}/calmodulin binding; and PxxP, motif for SH3 binding. (*b*) Nucleotide-exchange cycles of Sos and RasGRF1. Sos stimulates nucleotide exchange from Ras when its Rem and Cdc25 domains engage a nucleotide-bound Ras molecule at an allosteric site distal to the catalytic site. The Cdc25 domain of RasGRF1 is sufficient for Ras nucleotide-exchange activity.

from Ras in the presence of Sos ($5 \pm 2 \times 10^{-4}$ s^{-1} for 1 μM exchange factor) is comparable to the intrinsic rate of nucleotide release by isolated Ras and also to the observed nucleotide-release rate in the presence of Sos^{cat} W729E, a mutant that is impaired in binding allosteric Ras ($4.7 \pm 0.5 \times 10^{-4}$ s^{-1} for 1 μM exchange factor; Fig. 2) (16). In the presence of saturating concentrations of Ras^{Y64A}, a mutant of Ras that binds to the allosteric site of Sos but not to the active site (21), the nucleotide-release rate is increased over that of unstimulated Sos^{cat} (i.e., Sos in which the allosteric site is predominantly unoccupied) by a factor of 75 ($380 \pm 20 \times 10^{-4}$ s^{-1} for 1 μM exchange factor and 40 μM Ras^{Y64A}·GMPPNP; Fig. 2). Given these results, we refer to uncomplexed Sos^{cat} as "inactive" and Ras-bound Sos^{cat} as "active."

We also have found that the isolated Sos Cdc25 domain (Sos^{Cdc25}, residues 750–1,049) does not stimulate nucleotide release from Ras (the release rate is $1.5 \pm 0.2 \times 10^{-4}$ s^{-1} for 1 μM exchange factor; Fig. 2). A longer construct (residues 731–1,049, containing the Cdc25 domain plus 19 residues that link the Rem and Cdc25 domains) also is inactive, as are both constructs in the presence of Ras^{Y64A} (data not shown). We used circular dichroism spectroscopy to confirm that the inactivity of Sos^{Cdc25} does not result simply from lack of folding. Like Sos^{cat}, Sos^{Cdc25} is well folded, displaying a predominantly helical spectrum and a cooperative unfolding transition upon titration with chemical denaturant (Fig. 8, which is published as supporting information on the PNAS web site).

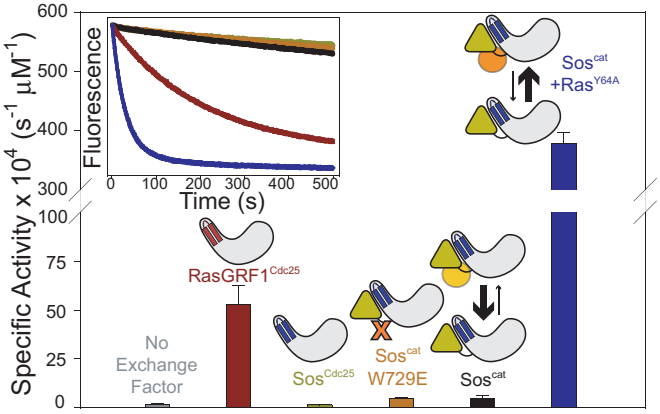

Fig. 2. Nucleotide-exchange assays. Nucleotide release from Ras is followed by a loss in fluorescence emission of mant-dGDP. RasGRF1^{Cdc25} increases the rate of nucleotide release from Ras relative to a control reaction. In contrast, the Sos Cdc25 domain alone and a mutant of Sos with the Rem and Cdc25 domains deficient in binding Ras at the allosteric site, Sos^{cat} W729E, lack substantial activity. Wild-type Sos^{cat} also is essentially inactive in the absence of allosteric activator. When GMPPNP-bound Ras^{Y64A}, a mutant of Ras that interacts only with the Sos allosteric site, is added at a saturating concentration, Sos^{cat} becomes maximally active. These reactions are carried out by using 0.1 μM substrate Ras·mant-dGDP, a concentration at which Ras·GDP does not interact significantly with the allosteric site of Sos (16).

Structures of Sos^{cat} and RasGRF1^{Cdc25} in the Absence of Ras. We crystallized Sos^{cat} (Rem-Cdc25) in the absence of Ras and determined its structure at 2.0-Å resolution (Table 1, which is published as supporting information on the PNAS web site). The overall structure of the Cdc25 domain of uncomplexed, inactive Sos^{cat} is similar to that of Ras-bound, active Sos^{cat} (rmsd of 1.1 Å in C_α positions). There are, however, localized conformational changes in the Cdc25 and Rem domains in the absence of Ras. In the Cdc25 domain, the helical hairpin, a critical Ras-binding element, is rotated inward by ≈10° in the structure of the uncomplexed Cdc25 domain of Sos^{cat} compared with its orientation in the Ras-bound structure (rmsd of 4.4 Å for helical hairpin C_α positions after superposition on the Cdc25 domain core; Fig. 3*a*). This conformational change is an *en bloc* movement of the helical hairpin with respect to the rest of the Cdc25 domain, as indicated by a distance difference matrix (Fig. 9*a*, which is published as supporting information on the PNAS web site). A similar rotation of the Rem domain also is observed.

We also determined the crystal structure of RasGRF1^{Cdc25} at 2.2-Å resolution (Table 1). The structure of the Cdc25 domain of RasGRF1 is very similar to that of Sos, consistent with the 30% sequence identity within the two Cdc25 domains (Fig. 7). The orientation of the helical hairpin of RasGRF1 resembles that of active Sos^{cat} (rmsd of 2.3 Å for the helical hairpins after superposition on the Cdc25 domain core; Fig. 3*b*) and is rotated outward relative to that of uncomplexed Sos^{cat} (rmsd of 5.5 Å for the helical hairpins after superposition on the Cdc25 domain core; Fig. 3*c*). Distance difference matrices confirm that the differences between the Cdc25 domains of RasGRF1 and inactive Sos^{cat} (Fig. 9*b*) are localized to the helical hairpin position

BIOCHEMISTRY

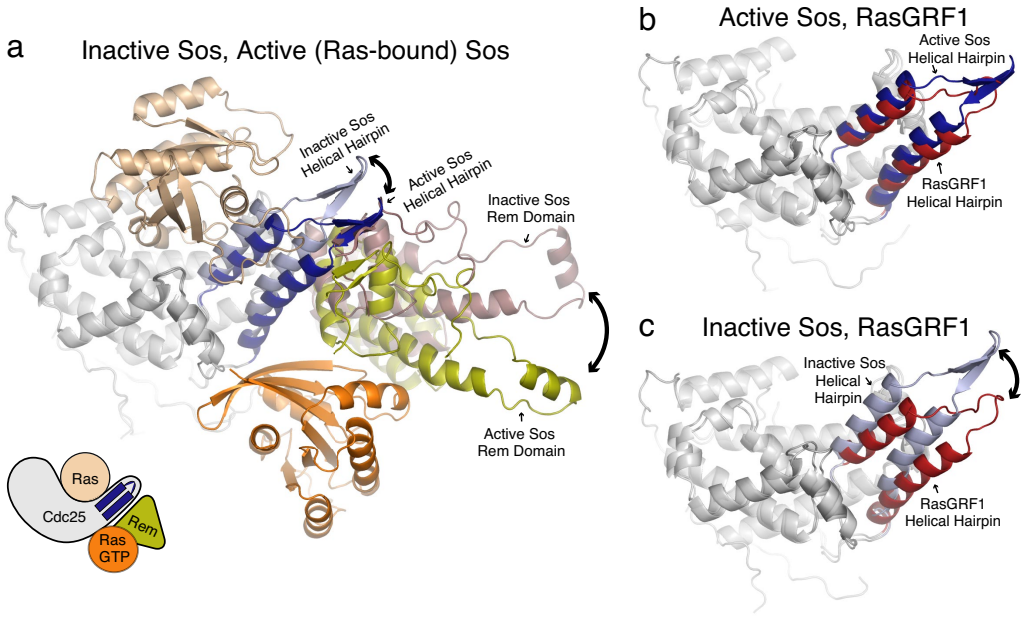

Fig. 3. Crystal structures of Sos^{cat} and $RasGRF1^{Cdc25}$. (*a*) Sos activation occurs through coordinated rotation of the helical hairpin and the Rem domain upon Ras binding to the allosteric site. The structures of uncomplexed Sos and Ras-bound Sos (15) are superposed on the Cdc25 domain core, excluding the helical hairpin, extended loops, and termini. Upon allosteric activation by Ras, the helical hairpin and the Rem domain pivot outward by 10°. (*b* and *c*) The Cdc25 domain of RasGRF1 has a conformation more similar to that of active Sos than that of inactive Sos.

relative to the rest of the Cdc25 domain, and that the conformation of $RasGRF1^{Cdc25}$ is more similar to that of active Sos^{cat} (Fig. 9*c*).

Structural Basis for the Allosteric Activation of Sos by Ras. Sos engages Ras at the catalytic site by binding Tyr-64 from the switch 2 region of Ras in a deep pocket abutting the helical hairpin (14), and the inability of Sos to release nucleotide from the Ras^{Y64A} mutant shows that this interaction is essential for Sos-catalyzed nucleotide exchange (21). In the structure of uncomplexed Sos^{cat}, the inward-rotated helical hairpin generates extensive steric clashes with Ras modeled at the active site, effectively blocking access to the Tyr-64 binding pocket and rendering uncomplexed Sos inactive (Fig. 4*a* and Fig. 10*a*, which is published as supporting information on the PNAS web site).

Upon binding to the Sos allosteric site, nucleotide-bound Ras pulls the Rem domain downward by ≈10° (Fig. 3*a*). The Rem and Cdc25 domains of Sos share an extensive interface, including a four-stranded β-sheet that incorporates two strands from the turn of the helical hairpin and two strands from the Rem domain. The structure of this β-sheet is unaltered in the uncomplexed (Fig. 11*a*, which is published as supporting information on the PNAS web site) and Ras-bound Sos structures (Fig. 11*b*), and so the position of the helical hairpin appears to be coupled strongly to the orientation of the Rem domain. When Ras binding to the allosteric site rotates the Rem domain, the helical hairpin is pulled along, opening the catalytic site for Ras (Figs. 4*b* and 10*b*). Another possible link between the Rem and Cdc25 domains of Sos is the hydrophobic interface between the Rem and Cdc25 domains, which has been shown by mutagenesis to be essential for Sos activity (21). A complex of Sos^{cat} bound to Ras at the allosteric site alone has not been crystallized. Because Sos^{cat} (Rem-Cdc25) requires occupation of the allosteric site for Ras interaction at the catalytic site (16), we believe that the activating conformational change is attributable to the Ras molecule at the allosteric site and not the one at the catalytic site. The rotation of the Rem domain when Ras is not bound to the allosteric site has been seen previously in a crystal structure of autoinhibited Sos in which the allosteric site is blocked by the DH and PH domains, but low resolution of the data (3.6 Å) precluded a definitive analysis (16).

Epac2, a Sos homolog that activates the Ras-related protein Rap1, is autoinhibited by regulatory domains that prevent Rap1 binding to the active site (22). Interestingly, the helical hairpin in the Cdc25 domain of inactive Epac2 is pivoted inward relative to that of active Sos, blocking the active site (Fig. 12, which is published as supporting information on the PNAS web site). As in Sos, the interaction between the helical hairpin of Epac2 and the Rem domain includes an interdomain β-sheet (Fig. 11*c*). A conformational switch driven by movements of the Rem domain and the helical hairpin thus appears to be a conserved feature among a subset of nucleotide-exchange factors for the Ras superfamily.

Structural Features That Underlie the Activity of RasGRF1 in the Absence of Allosteric Activation. The results discussed so far indicate that the helical hairpin of RasGRF1 is stable in the active conformation, whereas that of Sos is not. Strikingly, the helical hairpin of RasGRF1 is buttressed on either side by projections extending from the Cdc25 domain core, which we call flap1 and flap2 (Fig. 5*a*), whereas the helical hairpin of Sos interacts less closely with the corresponding flaps. The bulky side chains of Tyr-1048, Phe-1051, and Phe-1052 from flap1 of RasGRF1 interact with Ile-1210 and Ile-1214 from the helical hairpin (Fig. 5*b*). Sos contains smaller residues at this interface, including Pro-801, Leu-804, and Val-805 in flap1 and Val-964 and Thr-968 in the helical hairpin. When activated by allosteric Ras binding, the helical hairpin of Sos^{cat} is rotated away from flap1 (Fig. 5*c*). However, in the absence of allosteric Ras, the helical hairpin forms a tighter interface with flap1 (Fig. 5*d*). A similar collapse of the RasGRF1 helical hairpin to a Sos-like inactive conformation appears to be prevented by the bulky residues in the flap1-helical hairpin interface.

The link between flap2 and the helical hairpin of RasGRF1 is maintained by Arg-1160 and Arg-1165 in flap2 that bridge to Asp-1185 in the helical hairpin. Phe-1188 and Met-1181 from the

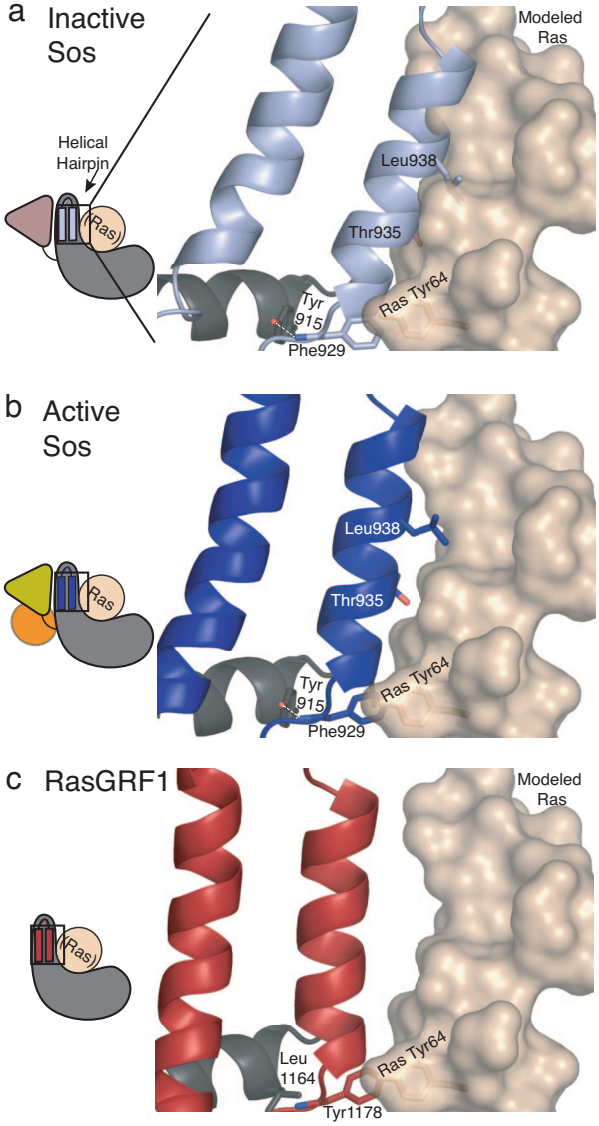

Fig. 4. Inward rotation of the helical hairpin toward the catalytic Ras binding site. (*a*) A cutaway view of the catalytic site of uncomplexed Sos shows that when Ras is docked in its binding site, it clashes extensively with the inward-rotated helical hairpin. The placement of Ras in the catalytic site is modeled from the Ras-bound Sos structure with Tyr-64 of Ras oriented correctly in its binding pocket (15). (*b*) Upon allosteric Ras binding, the Sos helical hairpin rotates outward, relieving the steric clashes with Ras at the catalytic site (1NVV) (15). The helical hairpin pivots around residue Tyr-915 from the Sos Cdc25 domain core, which hydrogen-bonds through its hydroxyl group to the amide nitrogen of Sos Phe-929 in the helical hairpin. (*c*) RasGRF1^{Cdc25} achieves a helical hairpin position compatible with Ras binding to the catalytic site and lacks the anchor/pivot point interaction for helical hairpin rotation, substituting Leu-1164 for Sos Tyr-915.

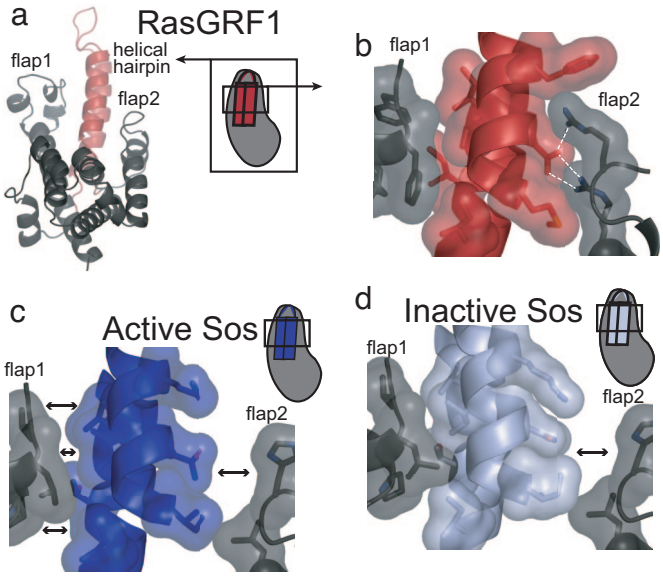

Fig. 5. The clamping of the helical hairpin. (*a*) View of RasGRF1 showing the helical hairpin (red), flap1, and flap2 (both gray). (*b*) A cutaway view through the catalytic Ras binding site of RasGRF1. A tight interface between flap1 and the helical hairpin of RasGRF1 is formed by bulky, hydrophobic residues (Phe-1052, Phe-1051, and Tyr-1048 in flap1, Ile-1214, and Ile-1210 in the helical hairpin). A salt-bridge network and hydrophobic interactions connect the helical hairpin with flap2 (Met-1181 and Phe-1188 bury Asp-1185 in the helical hairpin, bridging to Arg-1160 and Arg-1165 in flap2). (*c*) In the active conformation of Sos, the helical hairpin (dark blue) is similar in position to that of RasGRF1, but the interface with flap1 is not well packed (Val-805, Leu-804, and Pro-801 in flap1, Thr-964 and Val-968 in the helical hairpin). (*d*) In the absence of allosteric Ras binding, the helical hairpin of uncomplexed Sos (light blue) collapses inward to interact more closely with flap1. Neither active nor inactive Sos helical hairpins form close interactions with flap2 (Lys-939, Ile-932, and Asn-936 in the helical hairpin do not form contacts with His-911 and Leu-916 in flap2).

helical hairpin enclose the arginine residues in flap2 (Fig. 5*b*). In contrast, flap2 of Sos does not interact with the helical hairpin (Fig. 5 *c* and *d*). The residues that anchor flap1 and flap2 of RasGRF1 to the helical hairpin are conserved in RasGRF1 sequences but not in Sos sequences (Fig. 7).

To further analyze the significance of these structural features, we tested computationally the effects of swapping residues from the Cdc25 domain of RasGRF1 into the Cdc25 domain of Sos and vice versa. Residues differing in the two polypeptide chains were allowed either to retain their original identity or to "mutate" to the corresponding amino acid residue from the other protein. Monte Carlo-simulated annealing then was used to allow side chains to move while the backbone remained fixed. The energetic consequence of each substitution was calculated (23, 24) and used to determine whether a substitution move during the simulation was kept or discarded. In this way, the Sos or RasGRF1 sequence could accumulate substitutions that stabilize the observed backbone conformation in each simulation. Repetition of these simulations allowed the calculation of a substitution frequency for each residue, reflecting the number of times the wild-type residue swapped with the corresponding residue from the other protein in the low-energy sequences.

These computational experiments yield the striking result that the Sos structure acquires several buried residues from the RasGRF1 sequence with high frequency (Fig. 6*a*), whereas relatively few buried residues in RasGRF1 are replaced by their counterparts in Sos (Fig. 6*b*). In RasGRF1, the positions that switch to the Sos sequence are located in the Cdc25 domain core, remote from the helical hairpin. This outcome differs from the results for Sos, in which a large number of sequence swaps occur in the helical hairpin or in abutting regions of the Cdc25 domain.

These results indicate that RasGRF1 residues may be better than Sos residues at stabilizing the helical hairpin in the active backbone conformation. For example, active Sos acquires some high-frequency substitutions to RasGRF1 residues in the interface between flap1 and the helical hairpin. Sos residues Val-964, Thr-968, and Val-805 (Fig. 6*c*) are replaced with the corresponding residues in RasGRF1, Ile, Ile, and Phe, respectively. Presumably, the larger side chains more effectively fill the gap between the helical hairpin and flap1 in the active Sos confor-

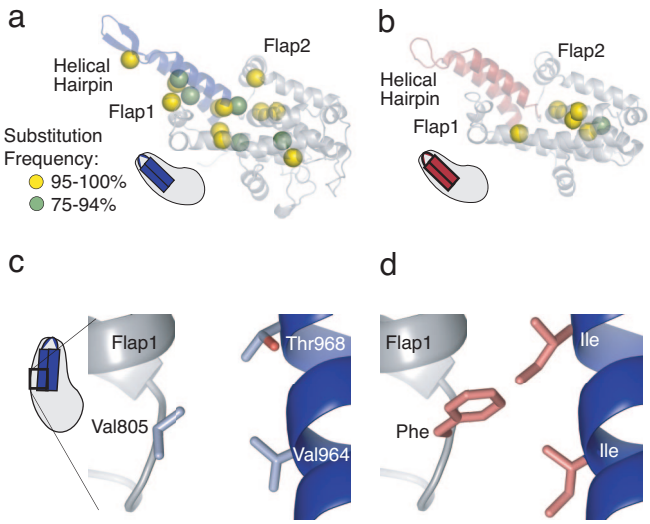

Fig. 6. Computational study of the effects of swapping residues from RasGRF1 and Sos. The number of times a given residue accumulated a conformation-stabilizing mutation in low-energy sequences from 100 separate Monte Carlo simulations is described by the substitution frequency. (*a* and *b*) C_α positions for buried residues that are swapped with high frequency are indicated (spheres) for Sos (*a*) and RasGRF1 (*b*). (*c* and *d*) Several Sos residues that substitute with high frequency are located in the flap1-helical hairpin interface (see also Fig. 5). (*c*) Wild-type Sos. (*d*) Substitutions from RasGRF1.

mation imposed during the simulations in the absence of the Rem domain and allosteric Ras (Figs. 5*c* and 6*d*). Interestingly, in a similar simulation with the inactive Sos backbone structure, this interface does not acquire RasGRF1 residues (Fig. 13, which is published as supporting information on the PNAS web site). This finding is consistent with the observation that the flap1-helical hairpin interface is more tightly packed in inactive Sos (Fig. 6*d*), and so bulky RasGRF1 residues would destabilize this conformation and be rejected as higher-energy changes. In other respects, the inactive Sos simulation is similar to that of active Sos.

The conformational switch used by Sos seems to occur at the expense of the conformational stability apparent in RasGRF1. For example Tyr-915 in Sos (Fig. 4), Phe-930, Tyr-796, Met-824, Glu-792, Tyr-974, and Asn-866, which interact with the base of the Sos helical hairpin and accommodate the conformational switch, mutate to RasGRF1 residues in almost every Sos simulation, whereas the corresponding residues in RasGRF1 remain unchanged.

Concluding Remarks

Sos and RasGRF1 are homologous exchange factors that contain Rem and Cdc25 domains. Biochemical characterization of RasGRF1 (17) had established that only the Cdc25 domain is required for Ras-specific nucleotide-exchange activity, and so the subsequent discovery that Sos is inactive without allosteric Ras binding to the Rem and Cdc25 domains was surprising (16). We now show that this functional distinction between Sos and RasGRF1 is reflected in the structures of the Cdc25 domains of the two proteins. The helical hairpin jutting out from the Cdc25 domain of Sos switches between conformations that either block or support Ras binding to the catalytic site. The open and active conformation of the Sos Cdc25 domain is induced allosterically by the binding of Ras to the distal site formed by the Rem and Cdc25 domains, causing a pivoting of the Rem domain upon allosteric Ras binding that is coupled to the pivoting of the helical hairpin relative to the Cdc25 domain core.

There is no structural information about the Rem domain of RasGRF1, and its function has not been fully explored. Previous studies have suggested that the Rem domain of RasGRF1 is regulatory in function, containing phosphorylation sites and PEST motifs (25–28). The level of activity we observe for the isolated Cdc25 domain of RasGRF1, although significantly greater than the intrinsic rate of nucleotide release from Ras, is much lower than the maximum rate observed for allosterically activated Sos^{cat}. At this time it is unknown whether RasGRF1 is truly less active than Sos or whether a binding partner will be found that triggers enhanced RasGRF1 activity.

Materials and Methods

Purification of Sos^{Cdc25}, Sos^{cat}, and $RasGRF1^{Cdc25}$. Sos^{cat} (Rem-Cdc25, human Sos1, residues 564-1049) and Sos^{Cdc25} (residues 750-1049) were purified as described for Sos^{cat} (15). $RasGRF1^{Cdc25}$ (murine RasGRF1, residues 1028–1262) was subcloned from cDNA into a pGEX-6P-3 vector with an N-terminal glutathione *S*-transferase affinity tag and purified essentially as described (11). A final Superdex 200 column (Amersham PharmaciaUppsala, Sweden) ensured homogeneity and exchanged the protein into buffer containing 200 mM NaCl. In contrast to previous reports (17), freezing and concentration did not affect $RasGRF1^{Cdc25}$ activity. RasGRF1 is insoluble at room temperature (11) but was soluble to >60 mg/ml on ice. A longer construct of RasGRF1 analogous to "$Cdc25^{Mm285}$" that includes 51 residues N-terminal to the Cdc25 domain (17) has comparable activity to $RasGRF1^{Cdc25}$ in our hands.

Nucleotide Exchange Assay. Nucleotide-exchange activity was measured by monitoring the decrease in fluorescence as labeled nucleotide was released from Ras (11). We used as the nucleotide 3′-*O*-*N*-methyl-anthraniloyl-2′-deoxy-guanosine-5′-diphosphate (mant-dGDP, Jena Bioscience, Jena, Germany) rather than mant-GDP to avoid artifacts caused by isomerization of the fluorescent label (18). The concentration of Ras was determined by colorimetric bicinchoninic acid (BCA) assay (Sigma, St. Louis, MO). The concentrations of Sos and RasGRF1 stock solutions were determined by A_{280} (29). Concentrations calculated by this method agreed with values generated by using the BCA assay. Reactions were initiated by rapid 1:1 mixing of 2 μM exchange factor ± Ras^{Y64A}·GMPPNP with 0.2 μM substrate, by using a stopped flow apparatus (RX2000; Applied Photophysics, Surrey, U.K.) linked to a Horiba Jobin Yvon (Edison, NJ) Fluoromax-3 fluorimeter. Reaction progress was monitored by fluorescence intensity at 430 nm of a 300-μl reaction after excitation at 370 nm. The samples, the stopped flow apparatus, and the cuvette were incubated at 15°C before reaction initiation. Excitation slits were fixed at 5 nm, and data were recorded every 0.5 s after integration over 0.05 s. Reactions were carried out for 9,207 seconds (the software limit) or 20 times the half-life of the nucleotide-exchange reaction. Data were obtained by averaging three consecutive runs with the same sample and then performed in triplicate on different days with different protein samples.

Data were analyzed with Prism 3 (Graphpad 3.0) and Sigmaplot (Systat Software, Inc., San Jose, CA) by fitting to a double exponential ($Y = A_0 + A_1e^{-k1\cdot t} + A_2e^{-k2\cdot t}$), where the higher-amplitude phase was the nucleotide-exchange rate and the invariant lower-amplitude phase was attributed to photobleaching and ignored. After fitting, the raw data for each reaction were normalized independently between 0 and 1, by using the formula $Y_{\text{normalized}} = (Y_{\text{raw}} - A_0)/(M - A_0)$, where A_0 represents the offset value from the exponential fit and M is the initial, maximum fluorescence.

Crystallization, X-Ray Data Collection, and Structure Solution. Crystals of Sos^{cat} were obtained by hanging drop-vapor diffusion by

mixing equal volumes of protein (50 mg/ml) and well solution (20% PEG 3350/0.2 M ammonium chloride). Crystals appeared overnight at 20°C. Crystals were cryoprotected by transfer to well solution including 20% glycerol for 5 min and then frozen in propane and kept at 100 K during data collection.

RasGRF1^{Cdc25} crystallized overnight at 4°C after mixing 1 μl of 10 mg/ml protein stock (in final buffer from purification with 5 mM tris(2-carboxyethyl)phosphine hydrochloride (TCEP) and 10% glycerol) and 1 μl of well solution (0.1 M sodium acetate, pH 5.2/3% PEG 4000/0.5% β-octyl glucoside). Cryoprotection was achieved by transferring crystals to well solution including 30% sucrose and flash-freezing in liquid nitrogen.

Crystallographic data (Table 1) were collected by using synchrotron radiation and reduced by using HKL2000 (30). Structures were solved by molecular replacement using PHASER (31). The search models for Sos^{cat} were the Cdc25 and Rem domains from Protein Data Bank entry 1NVV (15). The search model for solving the structure of RasGRF1^{Cdc25} was the isolated Cdc25 domain from Protein Data Bank entry 1NVV (15). Models were refined by using CNS (32) and O (33). Pymol was used for molecular illustrations (34).

Sequence Optimization by Monte Carlo Sampling. We calculated the substitution frequencies of Sos and RasGRF1 residues for the structures of active Sos, inactive Sos, and RasGRF1 by using published methods (23, 24). Side-chain rotamers were sampled for each sequence position on a given polypeptide backbone. The conformations were scored with an energy function dominated by packing interactions, hydrogen bonding, and solvation (23). A Metropolis Monte Carlo protocol combined with simulated annealing (24) with the coordinates for the crystal structures of inactive Sos, active Sos (1NVV) (15), and RasGRF1 was used to optimize the structures. At positions where the Sos and RasGRF1 sequences aligned and differed, the two different amino acid types were allowed. For all other positions, only the wild-type amino acid was considered, but different rotameric conformations were sampled. For each backbone, we performed 100 Monte Carlo runs, and the lowest-scoring sequences from 100 independent Monte Carlo simulations (with $\approx 2.5 \times 10^6$ amino acid or rotamer substitutions in each simulation) were used to compile substitution frequencies at each position.

Equilibrium Chemical Denaturation of Sos^{cat} and Sos^{Cdc25}. Sos^{Cdc25} or Sos^{cat} was diluted to concentrations of 50 or 40 μg/ml, respectively, into 0 or 9 M urea with 50 mM NaCl, 0.5 mM tris(2-carboxyethyl)phosphine hydrochloride (TCEP), and 10 mM acetate buffer (pH 5.5). Protein samples were equilibrated overnight at 25°C, and the circular dichroism (CD) signal and spectrum of each were recorded. Measurements were performed on an Aviv 62DS spectropolarimeter (Aviv Associates Inc., Lakewood, NJ). We report CD signal as the average of 120 points recorded every second at 222 nm. The lines represent fits generated from a three-state folding model, reflecting folded, intermediate, and unfolded states. In this case, the lines are used to guide the eye and are not interpreted quantitatively. CD spectra were taken with integration over 1 s, and those obtained in acetate buffer at pH 5.5 were identical those performed in 10 mM Tris at pH 8.0, a pH similar to that used for activity assays.

We thank Doug Lowy (National Cancer Institute, Bethesda, MD) for RasGRF1 cDNA; Jodi Gureasko, Nick Levinson, Bhushan Nagar, Oren Rosenberg, Xuewu Zhang, Olga Kuchment, and Steve Kazmirski for interesting discussions; and David King for mass spectrometry. We thank Corie Ralston, Gerry McDermott, and the scientists at beamlines 8.2.1 and 8.2.2 at the Advanced Light Source (supported by the Howard Hughes Medical Institute) for assistance. H.S. is supported by the Leukemia and Lymphoma Society. G.D.F is supported by the National Science Foundation's Graduate Research Fellowship Program, and T.K. is supported by the Sloan Foundation. D.B.-S. and S.M. are supported by National Institutes of Health Grants GM50945 (to S.M.) and CA55362 and CA28146 (to D.B.-S.), and J.K. is supported by the National Cancer Institute Grant R01 CA096504-02.

1. Vetter IR, Wittinghofer A (2001) *Science* 294:1299–1304.
2. Medema RH, de Vries-Smits AM, van der Zon GC, Maassen JA, Bos JL (1993) *Mol Cell Biol* 13:155–162.
3. Egan SE, Giddings BW, Brooks MW, Buday L, Sizeland AM, Weinberg RA (1993) *Nature* 363:45–51.
4. Gale NW, Kaplan S, Lowenstein EJ, Schlessinger J, Bar-Sagi D (1993) *Nature* 363:88–92.
5. Li N, Batzer A, Daly R, Yajnik V, Skolnik E, Chardin P, Bar-Sagi D, Margolis B, Schlessinger J (1993) *Nature* 363:85–88.
6. Buday L, Downward J (1993) *Cell* 73:611–620.
7. Mattingly RR, Macara IG (1996) *Nature* 382:268–272.
8. Jacquet E, Vanoni M, Ferrari C, Alberghina L, Martegani E, Parmeggiani A (1992) *J Biol Chem* 267:24181–24183.
9. Wei W, Schreiber SS, Baudry M, Tocco G, Broek D (1993) *Brain Res Mol Brain Res* 19:339–344.
10. Schweighoffer F, Faure M, Fath I, Chevallier-Multon MC, Apiou F, Dutrillaux B, Sturani E, Jacquet M, Tocque B (1993) *Oncogene* 8:1477–1485.
11. Lenzen C, Cool RH, Wittinghofer A (1995) *Methods Enzymol* 255:95–109.
12. Tian X, Gotoh T, Tsuji K, Lo EH, Huang S, Feig LA (2004) *EMBO J* 23:1567–1575.
13. Kim JH, Shirouzu M, Kataoka T, Bowtell D, Yokoyama S (1998) *Oncogene* 16:2597–2607.
14. Boriack-Sjodin P, Margarit S, Bar-Sagi D, Kuriyan J (1998) *Nature* 394:337–343.
15. Margarit SM, Sondermann H, Hall BE, Nagar B, Hoelz A, Pirruccello M, Bar-Sagi D, Kuriyan J (2003) *Cell* 112:685–695.
16. Sondermann H, Soisson SM, Boykevisch S, Yang SS, Bar-Sagi D, Kuriyan J (2004) *Cell* 119:393–405.
17. Lenzen C, Cool RH, Prinz H, Kuhlmann J, Wittinghofer A (1998) *Biochemistry* 37:7420–7430.
18. Guo Z, Ahmadian MR, Goody RS (2005) *Biochemistry* 44:15423–15429.
19. Chenna R, Sugawara H, Koike T, Lopez R, Gibson TJ, Higgins DG, Thompson JD (2003) *Nucleic Acids Res* 31:3497–3500.
20. Rost B, Yachdav G, Liu J (2003) *Nucleic Acids Res* 32:W321–W326.
21. Hall BE, Yang SS, Boriack-Sjodin PA, Kuriyan J, Bar-Sagi D (2001) *J Biol Chem* 276:27629–27637.
22. Rehmann H, Das J, Knipscheer P, Wittinghofer A, Bos JL (2006) *Nature* 439:625–628.
23. Kortemme T, Morozov AV, Baker D (2003) *J Mol Biol* 326:1239–1259.
24. Kuhlman B, Baker D (2000) *Proc Natl Acad Sci USA* 97:10383–10388.
25. Baouz S, Jacquet E, Accorsi K, Hountondji C, Balestrini M, Zippel R, Sturani E, Parmeggiani A (2001) *J Biol Chem* 276:1742–1749.
26. Yang H, Cooley D, Legakis JE, Ge Q, Andrade R, Mattingly RR (2003) *J Biol Chem* 278:13278–13285.
27. Baouz S, Jacquet E, Bernardi A, Parmeggiani A (1997) *J Biol Chem* 272:6671–6676.
28. Rechsteiner M, Rogers SW (1996) *Trends Biochem Sci* 21:267–271.
29. Gasteiger EHC, Gattiker A, Duvaud S, Wilkins MR, Appel RD, Bairoch A (2005) in *The Proteomics Protocols Handbook*, ed Walker J (Humana), pp 571–607.
30. Otwinowski Z, Minor W (1997) *Methods Enzymol* 276:307–326.
31. Storoni LC, McCoy AJ, Read RJ (2004) *Acta Crystallogr D* 60:432–438.
32. Brunger AT, Adams PD, Clore GM, DeLano WL, Gros P, Grosse-Kunstleve RW, Jiang JS, Kuszewski J, Nilges M, Pannu NS, *et al*. (1998) *Acta Crystallogr D* 54:905–921.
33. Kleywegt GJ, Jones TA (1996) *Acta Crystallogr D* 52:829–832.
34. DeLano WL (2002) *Curr Opin Struct Biol* 12:14–20.

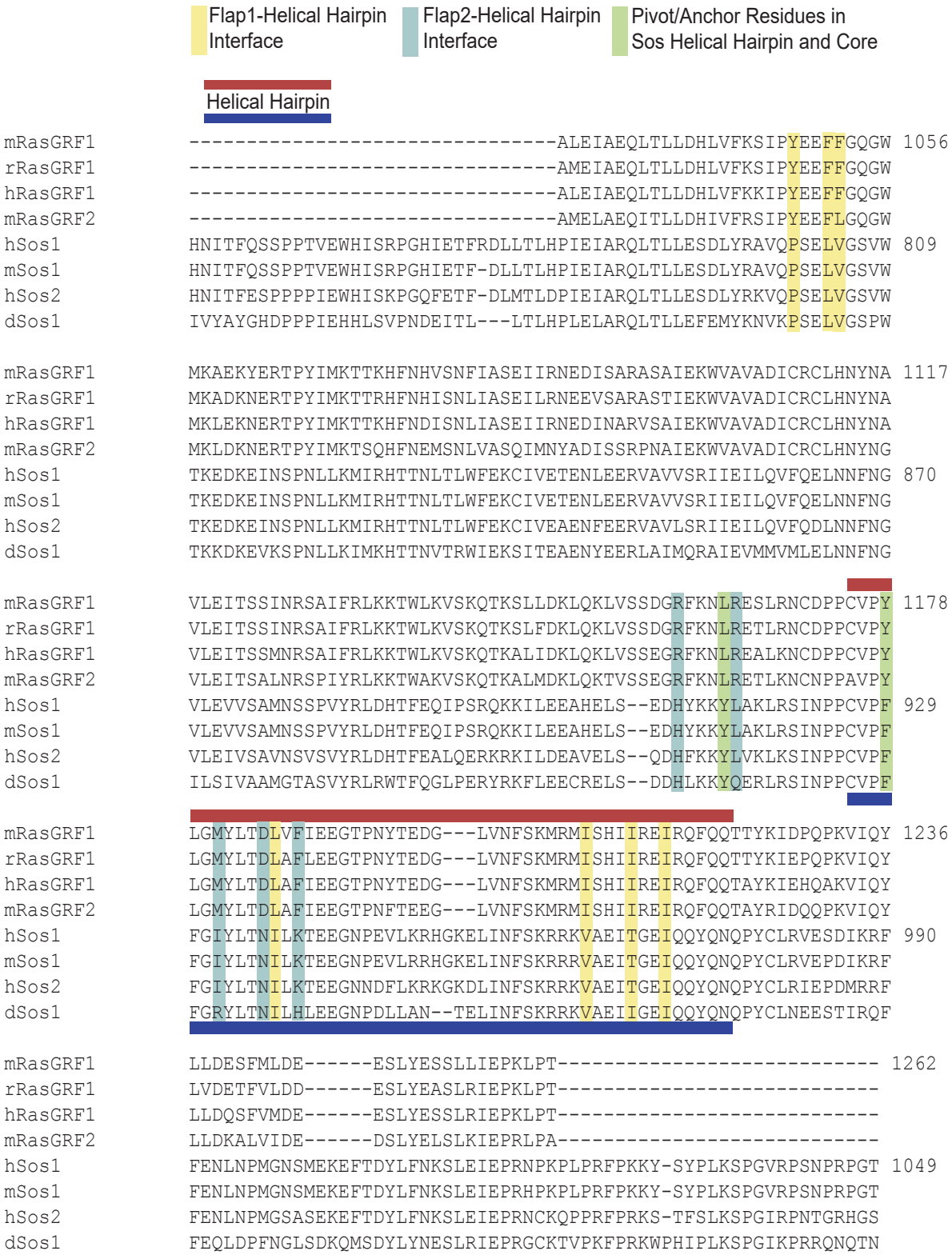

Fig. 7. Alignment of the Cdc25 domain sequences of Sos and RasGRF from mouse (m), human (h), rat (r), and fruit fly (d). The Cdc25 domains of mRasGRF1 and hSos1 (numbered) are 30% identical. Sequence elements that may be responsible for differences between Sos and RasGRF1 are highlighted. These residues are specific to RasGRF1 or Sos and are conserved in RasGRF1 and Sos sequences from different organisms.

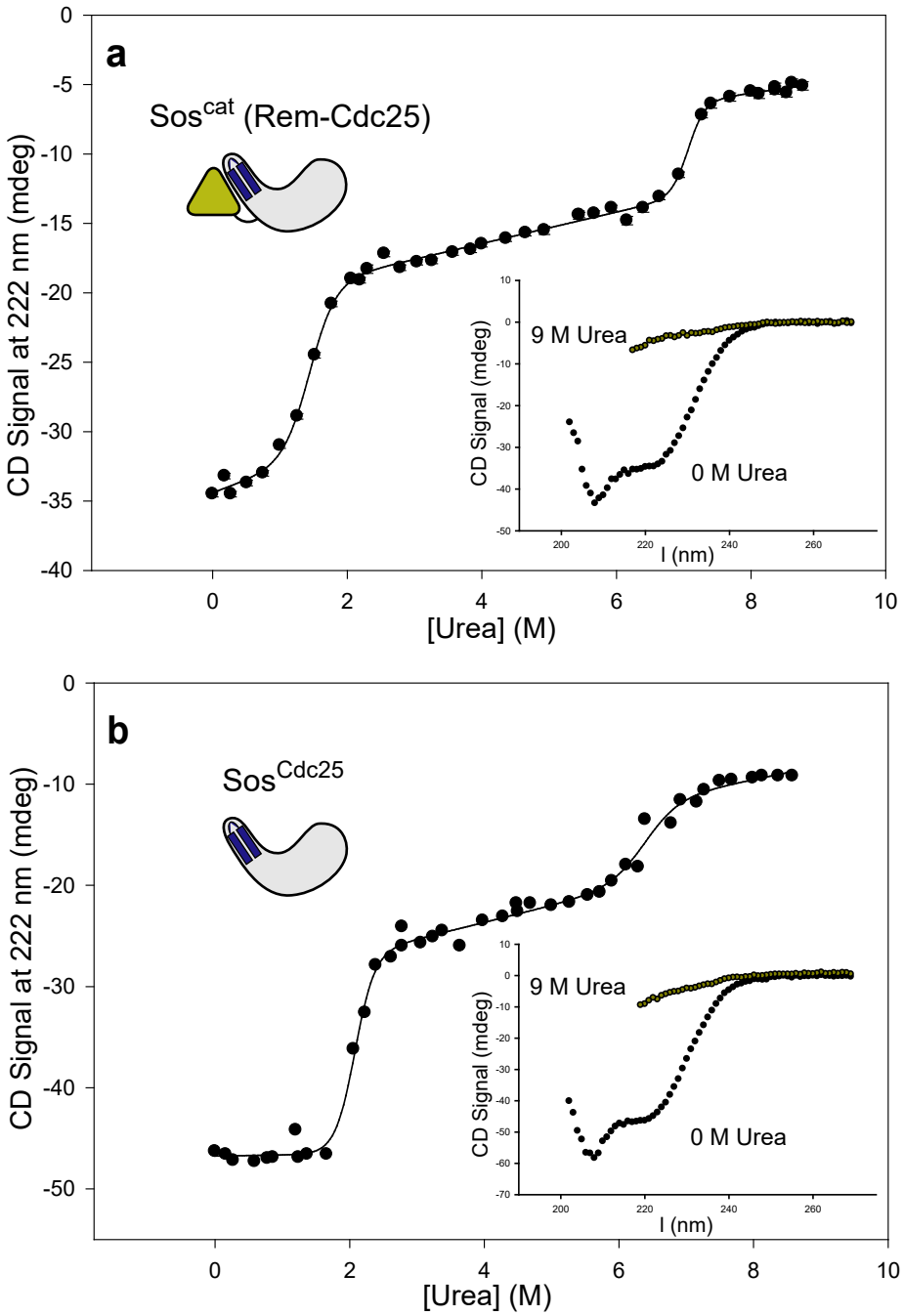

Fig. 8. Sos^{cat} and Sos^{Cdc25} have similar denaturation profiles and CD spectra. (a) Sos^{cat} displays two cooperative transitions upon equilibration in increasing amounts of urea. The CD spectrum in the absence of urea (Inset) reflects predominantly helical secondary structure, which disappears upon addition of urea to 9 M. (b) The cooperative denaturation profile and helical CD spectrum of Sos^{Cdc25} are similar to those of Sos^{cat}, indicating that Sos^{Cdc25} is well folded.

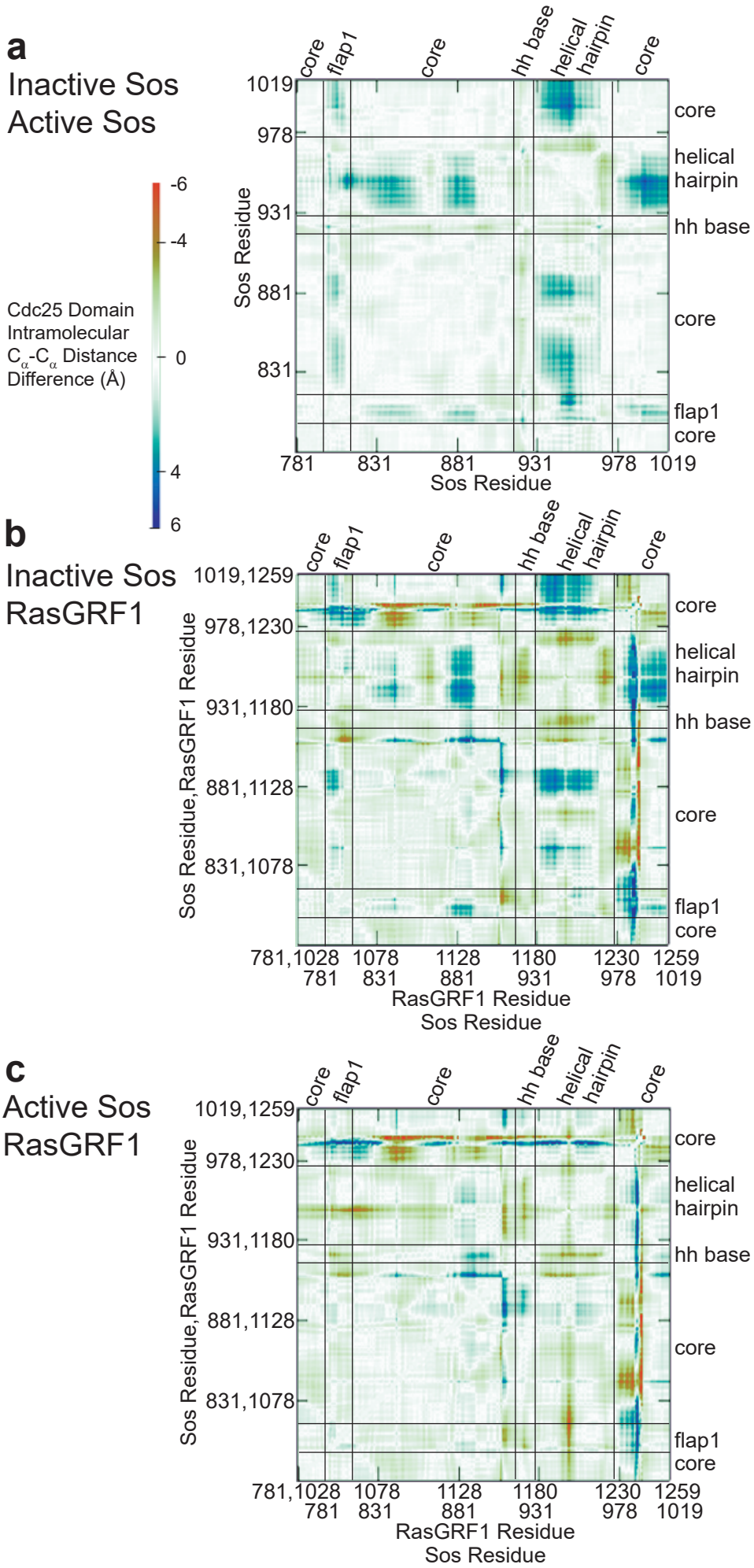

Fig. 9. Distance difference matrices show regions of change in intramolecular Cα positions in pairs of Sos and RasGRF1 Cdc25 domains. (a) Inactive and active Sos structures differ the most in helical hairpin position relative to the Cdc25 domain core. The base of the helical hairpin (hh base) similarly changes position with respect to the Cdc25 domain core. The flap1 region extending from the Cdc25 domain core to abut one side of the helical hairpin also changes position with respect to the helical hairpin and the rest of the Cdc25 domain core. (b) Like the comparison between inactive and active Sos, the comparison between inactive Sos and RasGRF1 shows different positioning of the helical hairpin and the flap region relative to the rest of the Cdc25 domain. (c) The position of the helical hairpin in RasGRF1 relative to the rest of the Cdc25 domain is more similar to that of active Sos.

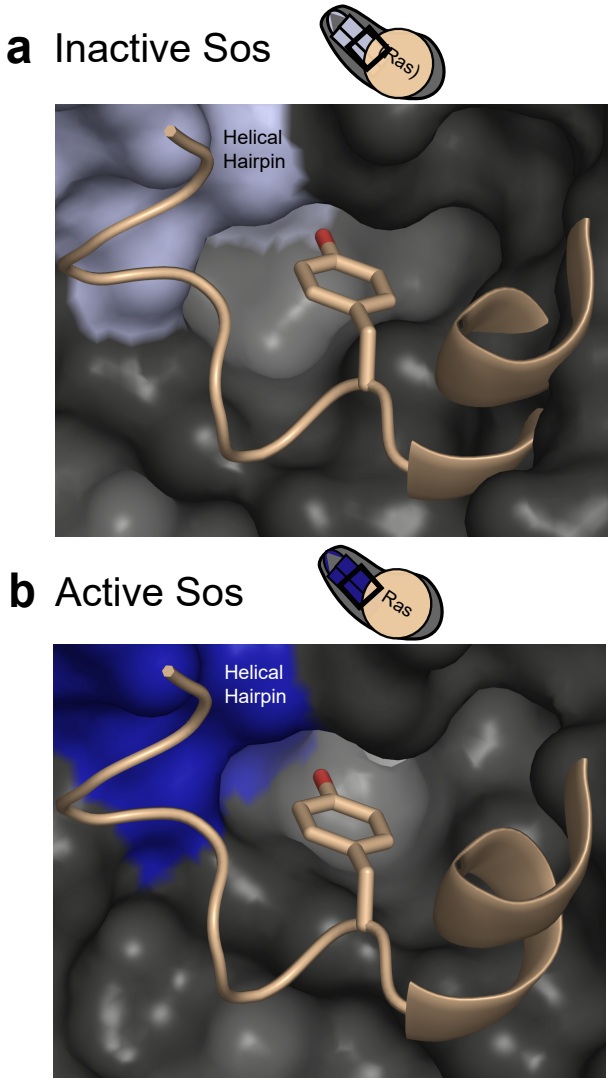

Fig. 10. Changes in the accessibility of the Ras Tyr-64 binding pocket in uncomplexed and Ras-bound Soscat. (a) Ras (from the active Sos structure, 1NVV) is docked into the catalytic site of uncomplexed Sos in a proper orientation with respect to the helical hairpin (as opposed to the best binding position of Tyr-64 shown in Fig. 4). In this orientation, catalytic site Ras clashes extensively with the core of the Cdc25 domain. Combination of both methods for docking Ras (from this view and that of Fig. 4) shows that binding of Tyr-64 and interaction with the helical hairpin, both critical for nucleotide exchange from Ras by Sos, are mutually exclusive in inactive Sos. (b) Upon allosteric Ras binding, steric clashes with Ras at the catalytic site are relieved.

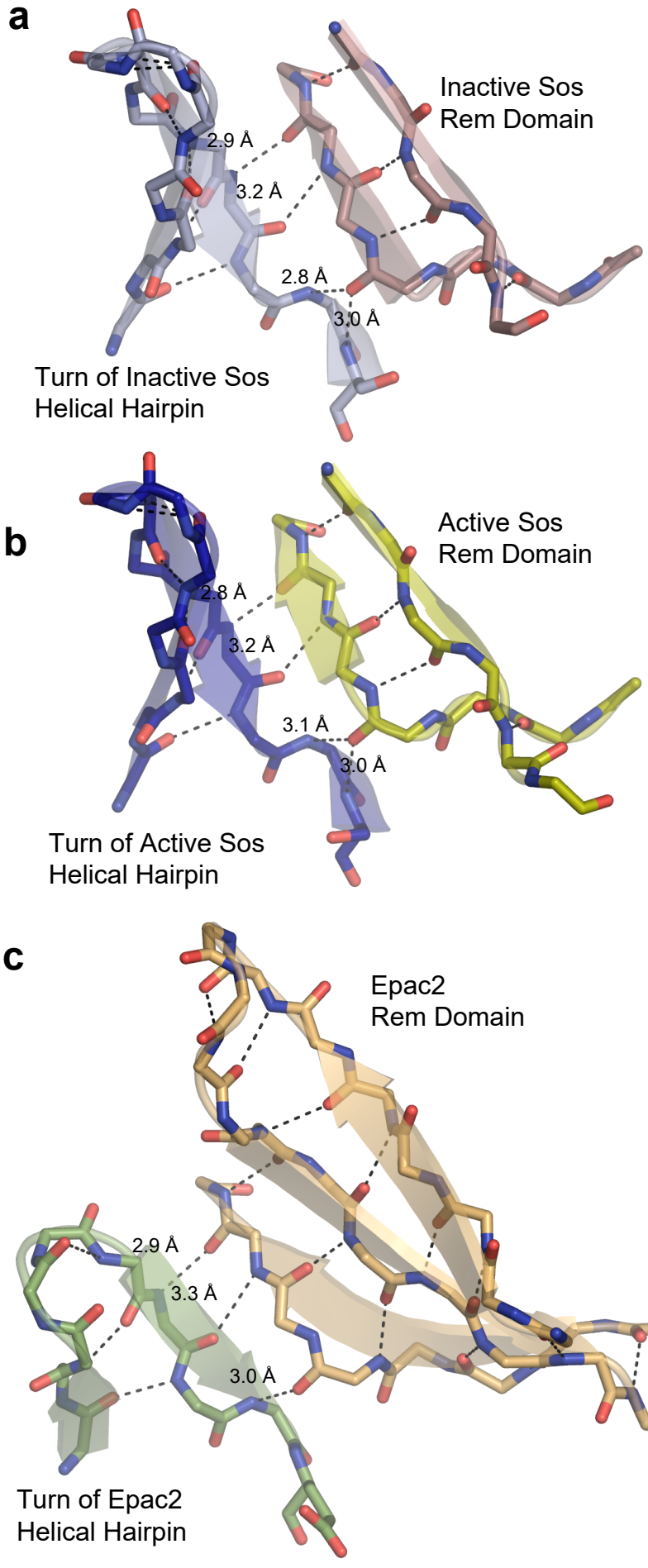

Fig. 11. β-Sheets couple the position of the helical hairpin to the position of the Rem domain in Sos and Epac2. (a) Two β-strands in the turn of the inactive Sos helical hairpin (light blue) and two strands in the Rem domain (light purple) form a four-stranded β-sheet across the two domains. Hydrogen-bond distances are indicated. (b) A similar β-sheet is formed by strands in the helical hairpin of active Sos (dark blue) and the Rem domain (yellow) despite significant motion of the Rem domain upon allosteric Ras binding. The hydrogen-bond distances indicate that this interaction is equally close in the active and inactive states. (c) Similar β-interactions between the helical hairpin (green) and Rem domain (orange) of Epac2 suggest that this mechanism of communication between the Rem and Cdc25 domains is conserved among other exchange factors.

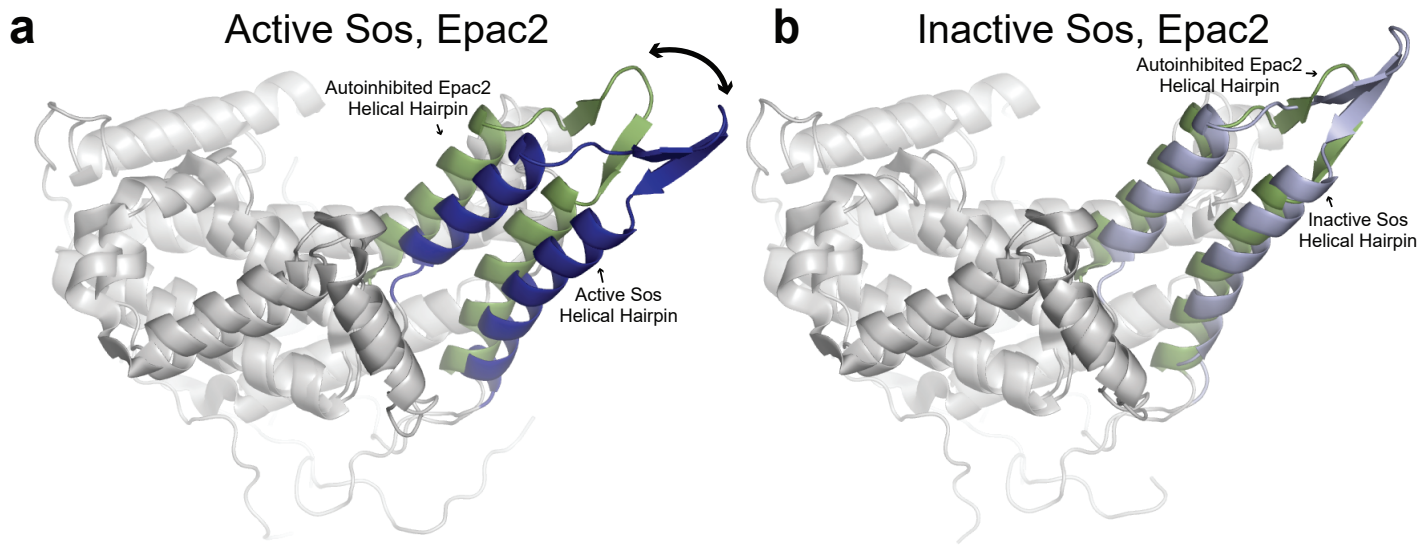

Fig. 12. The Cdc25 domain of Epac2 adopts an autoinhibited conformation similar to inactive Sos. (a) Relative to active Sos, the helical hairpin of autoinhibited Epac2 (from the full-length structure, green) is pivoted inward toward the catalytic site, with a conformation resembling inactive Sos (b).

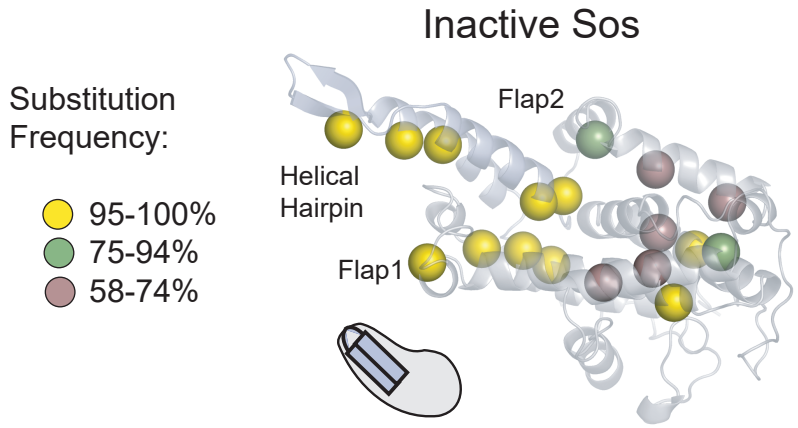

Fig. 13. Computational analysis of inactive Sos Cdc25 domain structure. As in Fig. 6, a computational analysis was performed where Sos or RasGRF1 residues could be exchanged at each position, this time using the inactive Sos backbone conformation. Results for inactive Sos are similar to those for active Sos except for the loss of several substitutions in the flap1-helical hairpin interface and an increase in lower-frequency substitutions to RasGRF1 residues in the Cdc25 domain core.